Research Square

Preprints are preliminary reports that have not undergone peer review.
They should not be considered conclusive, used to inform clinical practice,
or referenced by the media as validated information.

Textured Si Wafer-Assisted Fabrication of Stretchable Platinum Nanotube Network Electrodes for Flexible Piezoelectric Devices

Hee Yeon Jeon
Seoul National University of Science and Technology
Jeong Hyun Kim
Seoul National University of Science and Technology
Kyung-Shik Yoon
Seoul National University of Science and Technology
Hyeon Seong Kim
Seoul National University of Science and Technology
Jae Min Park
Seoul National University of Science and Technology
Kwanlae Kim
Seoul National University of Science and Technology
Sung-Tag Oh
Seoul National University of Science and Technology
Young-In Lee
youngin@seoultech.ac.kr

Seoul National University of Science and Technology

Research Article

Keywords: Platinum nanotube, Stretchable electrode, Textured silicon wafer, Electrospinning, Flexible piezoelectric device

Posted Date: September 8th, 2026

DOI: https://doi.org/10.21203/rs.3.rs-10883118/v1

License: This work is licensed under a Creative Commons Attribution 4.0 International License.
Read Full License

Additional Declarations: No competing interests reported.

Textured Si Wafer-Assisted Fabrication of Stretchable Platinum Nanotube Network Electrodes for Flexible Piezoelectric Devices

Hee Yeon Jeon[a], Jeong Hyun Kim[a], Kyung-Shik Yoon[a], Hyeon Seong Kim[a], Jae Min Park[a], Kwanlae Kim[b], Sung-Tag Oh[a,c] and Young-In Lee[a,c,*]

[a]*Department of Materials Science and Engineering, Seoul National University of Science and Technology, Seoul 01811, Republic of Korea*

[b]*Department of Manufacturing Systems and Design Engineering (MSDE), Seoul National University of Science and Technology, Seoul 01811, Republic of Korea*

[c]*The Institute of Powder Technology, Seoul National University of Science and Technology, Seoul 01811, Republic of Korea*

Corresponding author: Y.-I. Lee, Tel/Fax: +82-2-970-6646/+82-2-973-6657, Email: youngin@seoultech.ac.kr

Abstract

Flexible and stretchable electrodes are essential components for soft electronic devices that operate under repeated mechanical deformation. However, conventional metal thin-film electrodes often suffer from crack formation and electrical failure because of the mechanical mismatch between rigid metal layers and elastomeric substrates. In this study, we present a textured Si-assisted fabrication strategy for stretchable platinum nanotube (Pt-NT) network electrodes. Electrospun polyvinylpyrrolidone (PVP) nanofibers on a textured Si wafer were used as sacrificial one-

dimensional templates for Pt sputtering, enabling the formation of Pt-coated fibrous networks with controlled electrical continuity. Increasing the sputtering time increased the apparent Pt coating thickness and reduced the sheet resistance, indicating the development of interconnected Pt pathways. After thermal removal of the PVP template and transfer into polydimethylsiloxane (PDMS), the Pt-NT electrode exhibited a low sheet resistance of 7.55 Ω sq^{-1}. Under mechanical deformation, the Pt thin-film electrode showed electrical failure during bending and failed above 20% tensile strain, whereas the Pt-NT electrode maintained conductive pathways even at 100% strain. The Pt-NT electrode was further integrated with a $BaTiO_3$-PDMS piezoelectric composite layer, producing an output current of approximately 40 nA under an applied force of 25 N at 3 Hz. These results demonstrate that textured Si-assisted Pt-NT network electrodes can serve as deformable electrode platforms for flexible piezoelectric devices.

Keywords: Platinum nanotube; Stretchable electrode; Textured silicon wafer; Electrospinning; Flexible piezoelectric device

1. Introduction

Flexible and stretchable electrodes are key components in soft electronic systems, including wearable sensors, deformable displays, bio-integrated devices, and mechanical energy harvesting devices [1-3]. In these applications, electrodes are repeatedly subjected to bending, stretching, and local mechanical distortion while maintaining continuous electrical pathways [4-5]. Therefore, the electrode must provide not only high electrical conductivity but also mechanical stability under deformation. This requirement is particularly important for flexible piezoelectric devices, where unstable electrode contact or strain-induced electrical failure can directly reduce the reliability of the output signal [3, 6-8].

Metal thin films have been widely used as electrode layers because of their high intrinsic

conductivity and compatibility with conventional deposition processes [4, 9-10]. However, the mechanical mismatch between a rigid metal layer and an elastomeric substrate often induces crack formation during tensile deformation. Once cracks propagate through the metal film, the conductive pathway is interrupted, resulting in a rapid increase in resistance or electrical failure. Various structural designs, such as wavy layouts, mesh patterns, and serpentine interconnects, have been proposed to overcome this limitation [2, 11-14]. Although these approaches can improve deformability, they generally require complicated patterning or lithographic processes, which limits their practical use in simple and scalable fabrication of soft electrodes.

One-dimensional (1D) metallic nanostructures provide an alternative strategy for stretchable electrodes. In contrast to continuous thin films, a randomly distributed 1D network can maintain electrical conduction through interconnected pathways. The large aspect ratio of 1D nanostructures lowers the percolation threshold and increases the number of conductive junctions within the network [5, 15-21]. In addition to this network-level advantage, the small diameter of individual 1D nanostructures gives them intrinsically low flexural rigidity, allowing them to bend and deform more easily under external strain [22-24]. Therefore, a 1D metallic network can accommodate tensile deformation through a combination of local bending, sliding, rotation, and rearrangement of the nanostructures, rather than through the formation of large cracks as observed in continuous metal thin films. For this reason, metal nanowires, nanofibers, and nanotube networks have been actively investigated as electrode architectures for flexible and stretchable electronics [19, 25-26].

Among various metals, platinum (Pt) is attractive as an electrode material because of its high chemical stability, good electrical conductivity, and stable operation under repeated mechanical or electrical loading. However, the fabrication of Pt-based 1D network electrodes that combine electrical continuity, mechanical deformability, and transferability remains challenging. Conventional routes for preparing metallic nanofibers often involve electrospinning of metal precursor/polymer composite fibers followed by calcination and reduction [27-29]. These processes can cause pore formation, volume shrinkage, and structural damage during polymer decomposition and oxide reduction.

Direct deposition of metals onto electrospun polymer nanofibers is a simpler and more versatile approach [30-34]. Nevertheless, when polymer nanofibers are placed on a flat substrate, sputtered metal is preferentially deposited on the exposed upper surface of the fibers, while the fiber-substrate contact region remains less accessible to the incoming metal flux. This asymmetric deposition can lead to nanotrough-like structures rather than mechanically robust tubular networks. In addition, strong contact between the fibrous network and a flat substrate can make subsequent transfer to an elastomeric substrate less effective. Therefore, an appropriate supporting substrate is required not only for metal deposition around the nanofiber template, but also for retaining the 1D network morphology during transfer into an elastomer.

To address these limitations, a textured Si-assisted electrospinning/sputtering approach is proposed for constructing Pt nanotube network electrodes. In this approach, electrospun PVP nanofibers on a textured Si wafer serve as sacrificial 1D templates for Pt deposition. The textured surface is designed to reduce the direct contact area between the polymer nanofibers and the substrate, thereby providing more accessible space for Pt deposition around the fibrous template during sputtering. This configuration is also advantageous for the subsequent embedding and release of the Pt-based network into a PDMS substrate, because the reduced contact area can facilitate transfer while preserving the interconnected 1D architecture. Another important feature of this approach is that the amount of Pt deposition can be controlled by sputtering time without changing the overall fibrous network structure. Sufficient Pt deposition is necessary to form electrically continuous pathways and to reduce the effective sheet resistance of the network, whereas excessive structural damage or collapse of the 1D framework should be avoided. Thus, the textured Si-assisted sputtering process is expected to provide a practical route for preparing Pt nanotube network electrodes that combine network continuity, mechanical deformability, and compatibility with elastomer-supported flexible devices.

Based on this concept, the present study focuses on the fabrication of PDMS-embedded Pt nanotube network electrodes and their evaluation as flexible and stretchable electrodes. The formation

of Pt-coated PVP nanofiber networks on a textured Si wafer is first examined as a function of sputtering time to clarify the relationship between Pt deposition, fiber diameter, and sheet resistance. The structural evolution after thermal removal of the PVP template is then analyzed to confirm whether the 1D Pt-based network can be retained before transfer into PDMS. Conventional Pt thin-film electrodes are used as a control to clarify the effect of the 1D nanotube network architecture on deformation-induced electrical instability. Finally, the Pt nanotube network electrode is integrated with a $BaTiO_3$-PDMS piezoelectric composite layer to examine its applicability as a deformable electrode for flexible piezoelectric devices.

2. Experimental procedure

2.1. Fabrication of Pt nanotube network electrodes

Polyvinylpyrrolidone (PVP; M_w = 1,300,000 g mol^{-1}; Sigma-Aldrich, USA) was used as a sacrificial polymer template for the fabrication of Pt nanotube network electrodes. A PVP solution was prepared by dissolving 0.5 g of PVP in a mixed solvent composed of 2 g of anhydrous ethanol and 3 g of deionized water, corresponding to a PVP concentration of 10 wt% relative to the solvent mass. The solution was magnetically stirred at room temperature until PVP was completely dissolved. The prepared PVP solution was loaded into a 10 mL plastic syringe connected to a 30-gauge needle through a polymer tube. PVP nanofibers were electrospun directly onto a 2 cm × 2 cm textured Si wafer chip cut from a commercial textured Si wafer (210 mm × 210 mm, Yixing JS Solar Co., Ltd., China), which was used as a grounded collector. The electrospinning process was conducted at an applied voltage of 20 kV, a tip-to-collector distance of 13 cm, and a feeding rate of 0.4 mL h^{-1} for 1 min. Here, the textured Si wafer was used to reduce the contact area between the electrospun PVP nanofibers and the substrate, thereby facilitating Pt deposition around the fibrous template during the subsequent sputtering process.

Pt was deposited onto the electrospun PVP nanofiber network by sputtering for 10, 20, and 30

min using a Pt target (99.999% purity, RND Korea, Korea). Sputtering was performed at a base pressure of 2×10^{-5} Torr, a working pressure of 15 mTorr, and a power of 150 W. The Pt-coated PVP nanofibers were then subjected to thermal treatment at 500 °C for 3 h at a heating rate of 5 °C min^{-1} in air to remove the PVP template. As a result, a Pt nanotube network was obtained on the textured Si wafer. To fabricate the elastomer-supported electrode, polydimethylsiloxane (PDMS; Sylgard 184, Dow Corning, USA) resin and curing agent were mixed at a weight ratio of 10:1. The PDMS mixture was poured onto the Pt nanotube network formed on the textured Si wafer and cured at 80 °C for 2 h in a vacuum oven. After curing, the PDMS substrate embedded with the Pt nanotube network was carefully peeled off from the textured Si wafer. The resulting electrode is hereafter referred to as the Pt-NT electrode. For comparison, a Pt thin-film electrode, hereafter referred to as the Pt-TF electrode, was prepared by directly sputtering Pt onto a PDMS substrate for 30 min under the same sputtering conditions. The overall fabrication process of the Pt-NT electrode is schematically illustrated in Fig. 1a and 1c.

2.2. Fabrication of flexible piezoelectric devices

Flexible piezoelectric devices were fabricated by integrating the Pt-NT electrodes with a $BaTiO_3$ (BTO; average diameter = 200 nm; US Research Nanomaterials, USA)-PDMS piezoelectric composite layer. BTO nanoparticles were first dispersed in ethyl alcohol by ultrasonication for 30 min. PDMS resin was then added to the BTO/ethyl alcohol dispersion to prepare a BTO-PDMS composite solution with a BTO content of 30 wt% relative to PDMS. The mixture was further ultrasonicated to obtain a homogeneous dispersion. The BTO-PDMS dispersion was placed on a hot plate and stirred at 300 rpm and 50 °C until ethyl alcohol was completely evaporated. Subsequently, a curing agent was added to the BTO-PDMS mixture at a PDMS resin-to-curing agent weight ratio of 10:1. The resulting composite paste was spin-coated onto the Pt-NT electrode at 500 rpm for 1 min. Before spin coating, copper wires were attached to the electrode using silver paste to enable electrical connection. The coated electrode was pre-cured at 80 °C for 10 min in a vacuum oven. Two pre-cured electrodes were

then stacked face-to-face with the BTO-PDMS composite layers in contact with each other, followed by final curing at 80 °C for 2 h. After curing, the fabricated flexible piezoelectric device was electrically poled using a high-voltage amplifier (10/10B-HS, Trek, USA) under a DC electric field of 8 kV mm^{-1} for 24 h in silicone oil (SHINETSU, Japan) to align the dipoles in the BTO-PDMS composite layer. The overall fabrication process of the BTO-PDMS piezoelectric device is schematically illustrated in Fig. 1b and 1d.

2.3. Characterization and electrical measurements

The morphology of the electrospun PVP nanofibers, Pt-coated PVP nanofibers, Pt nanotube networks, and fabricated electrodes was observed using field-emission scanning electron microscopy (FE-SEM; JSM-6700F, JEOL, Japan). The elemental distribution of Pt was analyzed by energy-dispersive X-ray spectroscopy (EDS) attached to the FE-SEM system. The average diameter of the nanofibers was determined from FE-SEM images using ImageJ software based on 200 diameter measurements.

The sheet resistance of the Pt-coated nanofiber networks was measured using a non-contact sheet resistance measurement system (EC-80P, Napson Corporation, Japan) to examine the formation of conductive Pt pathways as a function of sputtering time. The sheet resistance of the transferred Pt-coated PVP nanofiber electrode and thermally treated Pt-NT electrode was also measured using the same non-contact system. For the fabricated Pt-NT and Pt-TF electrodes, copper wires were attached to the electrodes using silver paste, and the electrical resistance was measured using a two-terminal configuration. The mechanical reliability of the electrodes was evaluated by bending and stretching tests using a micro-fatigue tester (E3000LT, Instron, USA). The bending test was performed for 1,000 cycles at a bending radius of 5 mm and a frequency of 1/8 Hz. The stretching test was carried out by increasing the tensile strain from 10% to 100%. During the bending tests, the resistance was measured both in the bent state and after release of bending stress. The resistance change after release was

expressed as $\Delta R/R_0$ (%), whereas the resistance measured in the bent state was plotted directly. During stretching tests, the resistance variation was expressed as R/R_0, where R_0 and R are the initial resistance and the resistance under tensile strain, respectively.

The surface morphology and roughness of the electrodes after mechanical deformation were further analyzed using a 3D surface confocal laser scanning microscope (LSM 800, Carl Zeiss, Germany). The surface roughness parameters, including R_a and S_a, were obtained from the measured surface profiles. The piezoelectric output current of the flexible piezoelectric device was measured using a source meter (2612B, Keithley Instruments, USA) under periodic compressive loading. The periodic force was applied using a pushing tester (JIPT-100, Junil Tech, Korea) equipped with a 10 mm × 10 mm pushing tip. The output current was recorded under different applied forces of 5 to 25 N and pushing frequencies of 1 to 3 Hz.

3. Results and Discussion

3.1. Textured Si-assisted fabrication and structural evolution of Pt nanotube network electrodes

As schematically illustrated in Fig. 1a, the fabrication of the Pt-NT electrode begins with the formation of electrospun PVP nanofibers on a textured Si wafer. The PVP nanofiber network serves as a sacrificial one-dimensional template for subsequent Pt deposition. Fig. 2 shows the FE-SEM images of the as-spun PVP nanofibers and Pt-coated PVP nanofibers prepared with different sputtering times. The electrospun PVP nanofibers were randomly distributed over the textured Si wafer while maintaining a continuous fibrous network. Such an interconnected polymer network is suitable as a template for constructing a deformable conducting architecture.

After Pt sputtering, the fibrous morphology was retained without severe collapse or agglomeration. With increasing sputtering time, the Pt-coated nanofibers became progressively thicker, suggesting the gradual deposition of Pt onto the PVP nanofiber template. Although sputtering is generally a line-of-sight deposition process [30, 33], the textured Si wafer was used to reduce the

direct contact area between the nanofibers and the substrate. This configuration is expected to provide more accessible space for Pt deposition around the fibrous template than a flat substrate. Therefore, the morphological evolution observed in Fig. 2 supports the use of the textured Si-assisted process for preparing Pt-coated PVP nanofiber networks, which can be subsequently converted into Pt nanotube networks by removing the PVP template.

The structural evolution observed in Fig. 2 was quantitatively analyzed and correlated with the electrical response of the Pt-coated PVP nanofiber networks, as shown in Fig. 3. The average diameter of the pristine PVP nanofibers was 258 nm. After Pt sputtering for 10, 20, and 30 min, the average diameter increased to 304, 341, and 365 nm, respectively. Assuming that Pt was deposited around the nanofiber template, the apparent Pt coating thickness was estimated to be approximately 23, 42, and 54 nm for sputtering times of 10, 20, and 30 min, respectively. This gradual increase in diameter indicates that Pt was progressively deposited onto the PVP nanofiber template with increasing sputtering time.

More importantly, the increase in the estimated Pt coating thickness was accompanied by a marked decrease in sheet resistance. The sheet resistance decreased sharply when the sputtering time was increased from 10 to 20 min, whereas a more gradual decrease was observed between 20 and 30 min. This behavior suggests that the initial stage of Pt sputtering mainly promotes the development of electrically connected Pt coatings along the nanofiber surface. Once conductive pathways begin to form within the fibrous network, further sputtering contributes to the formation of a thicker and more continuous Pt coating, as well as more stable inter-fiber junctions, resulting in a smaller additional decrease in sheet resistance.

It should be noted that the estimated Pt coating thickness was calculated from the change in average fiber diameter and therefore represents an apparent value rather than a directly measured wall thickness. Nevertheless, the correlation among increased fiber diameter, increased apparent Pt coating thickness, and decreased sheet resistance demonstrates that sputtering time is a key parameter for controlling the electrical continuity of the Pt-coated nanofiber network. Based on these results, a

sputtering time of 30 min was selected for the subsequent fabrication of Pt nanotube network electrodes. The structural evolution of the Pt-coated nanofiber network after removal of the PVP template is discussed below.

The structural evolution of the Pt-coated PVP nanofiber network after thermal removal of the polymer template is shown in Fig. 4. Before thermal treatment, the sputtered sample exhibited a continuous fibrous network on the textured Si wafer. The EDS mapping images show that Pt was distributed along the nanofiber network, indicating that Pt was deposited on the electrospun PVP template rather than simply forming a continuous film on the exposed textured Si wafer surface. At this stage, however, the structure should be regarded as a Pt-coated PVP nanofiber network because the insulating polymer template remains inside the coated fibers. After thermal treatment at 500 °C for 3 h, the overall one-dimensional network morphology was retained. This result indicates that the Pt coating developed during sputtering was sufficiently continuous to preserve the fibrous framework after removal of the PVP template. As discussed in Fig. 3, the apparent Pt coating thickness for the sample sputtered for 30 min was estimated to be approximately 54 nm from the increase in average fiber diameter. Although local variation in wall thickness is expected in a sputtered fibrous network, this estimated value is in reasonable agreement with the wall-like Pt framework observed after thermal treatment. Therefore, this thermal treatment enabled the formation of a Pt nanotube network from the Pt-coated PVP nanofiber template while largely maintaining the original one-dimensional architecture.

The thermal treatment is important not only for structural conversion but also for electrical network formation. To directly evaluate the effect of thermal treatment on the electrical conductivity of the network, both the Pt-coated PVP nanofiber electrode and the thermally treated Pt-NT electrode were transferred onto PDMS substrates, and their sheet resistances were measured. The Pt-coated PVP nanofiber electrode without thermal treatment exhibited a relatively high sheet resistance of 213.45 Ω sq^{-1}, whereas the thermally treated Pt-NT electrode showed a substantially lower sheet resistance of 7.55 Ω sq^{-1}, corresponding to an approximately 28-fold decrease. This pronounced reduction in sheet

resistance indicates a significant improvement in electrical connectivity after thermal conversion of the Pt-coated PVP nanofibers into the Pt-NT network. If the Pt-coated PVP nanofibers were used without thermal treatment, the remaining PVP core could act as an insulating component and reduce the effective electrical connection between adjacent Pt-coated fibers, particularly at inter-fiber junctions. In contrast, removal of the PVP template allows the Pt framework and inter-fiber junctions to contribute more effectively to network conduction. This structural conversion can account for the much lower resistance of the thermally treated Pt-NT electrode compared with the Pt-coated PVP nanofiber electrode. Thus, the results in Fig. 4 provide the structural basis for the improved electrical response of the Pt-NT network and for the subsequent fabrication of PDMS-embedded stretchable electrodes.

The thermally treated Pt-NT network was transferred onto a PDMS substrate to fabricate a flexible and stretchable electrode, as shown in Fig. 5. During this process, the PDMS precursor was poured onto the Pt-NT network formed on the textured Si wafer, followed by curing and peeling from the substrate. The digital image and FE-SEM observation show that the Pt-NT network was embedded near the surface of the PDMS substrate while retaining its interconnected fibrous morphology (Fig. 5a, b). The corresponding EDS mapping shows that Pt was distributed along the network structure after transfer, indicating that the Pt-NT framework was largely retained during the embedding and release process. For comparison, a Pt-TF electrode was prepared by direct sputtering of Pt onto a PDMS substrate for 30 min under the same sputtering conditions. Unlike the Pt-NT electrode, the Pt-TF electrode exhibited a continuous film-like conducting layer on the elastomer surface (Fig. 5e, f). Therefore, Fig. 5 clearly distinguishes the two electrode architectures used in this study: a one-dimensional Pt-NT network partially embedded in PDMS and a two-dimensional Pt thin film formed on PDMS. This structural difference is important for the subsequent evaluation of mechanical reliability. In the Pt-NT electrode, the interconnected fibrous pathways and partial embedding in the elastomer can allow the conducting network to accommodate deformation through local bending, sliding, and rearrangement of the network structure. In contrast, the Pt-TF electrode is more likely to concentrate tensile strain within the continuous metal layer, leading to crack formation and

interruption of the conductive pathway. Thus, the electrode structures shown in Fig. 5 provide the basis for comparing the electrical stability of the Pt-NT and Pt-TF electrodes under bending and stretching deformation.

3.2. Electrical and mechanical reliability of Pt-NT electrodes under deformation

The electrical stability of the Pt-NT electrode under mechanical deformation was evaluated and compared with that of the Pt-TF electrode, as shown in Fig. 6. As discussed in the previous section, the two electrodes have distinctly different conducting architectures. The Pt-NT electrode consists of an interconnected one-dimensional network embedded near the surface of PDMS, whereas the Pt-TF electrode has a continuous two-dimensional metal film on the elastomer substrate. Therefore, their resistance responses under bending and stretching provide direct insight into the effect of electrode architecture on deformation-induced electrical instability.

During cyclic bending, the Pt-NT electrode maintained electrical conduction even under applied bending stress. The resistance increase was relatively small during the initial cycles and became more pronounced after repeated bending (Fig. 6a). Although the percentage increase became large after extended bending cycles, the resistance measured in the bent state remained within a measurable range for the Pt-NT electrode, indicating that the conducting network was not completely open-circuited. This behavior suggests that the interconnected Pt-NT pathways can accommodate bending deformation while preserving electrical contact within the network. In contrast, the Pt-TF electrode showed electrical failure under bending stress after only a small number of cycles. When the electrode was bent, the resistance rapidly increased, and the current pathway was interrupted after approximately 10 cycles (Fig. 6b). Interestingly, the resistance recovered after release of the bending stress. This reversible recovery indicates that the Pt thin film was not completely destroyed during the bending test. Instead, bending likely induced temporary crack opening or separation of conducting regions in the Pt film, and these disconnected regions came back into contact when the bending stress

was removed. Nevertheless, such deformation-dependent electrical failure is undesirable for flexible electrodes, because the electrode should maintain stable conduction while the device is under mechanical deformation, not only after release.

The difference between the Pt-NT and Pt-TF electrodes became more evident under tensile stretching (Fig. 6c). The Pt-TF electrode failed when the applied strain exceeded 20%, indicating that the continuous Pt film could not maintain an uninterrupted conducting pathway under large tensile deformation. This behavior is attributed to strain concentration in the rigid metal film and crack propagation across the conducting layer. By contrast, the Pt-NT electrode maintained electrical conductivity even at 100% strain. Although its resistance increased with increasing strain, the conducting pathway was not completely interrupted. These results demonstrate that the Pt-NT network architecture provides a more stable electrical pathway under both bending and stretching deformation than the Pt thin-film architecture. The improved stability is attributed to the interconnected one-dimensional network and its partial embedding in the PDMS substrate, which can accommodate deformation through local bending, sliding, and rearrangement of the fibrous pathways. Therefore, the Pt-NT electrode is more suitable for deformable electronic devices that require stable electrical conduction under mechanical deformation.

To clarify the origin of the different electrical responses observed in Fig. 6, the surface morphologies of the Pt-NT and Pt-TF electrodes were examined before and after 1,000 cycles of bending, as shown in Fig. 7. The Pt-NT electrode retained its interconnected fibrous network after bending, and no large cracks or severe delamination were observed on the electrode surface. This structural stability is consistent with the stable electrical conduction of the Pt-NT electrode during bending. The one-dimensional network can accommodate mechanical deformation through local bending and rearrangement of the fibrous pathways, thereby reducing the probability of complete pathway interruption.

In contrast, the Pt-TF electrode showed distinct crack formation after bending. Because the Pt-TF electrode consists of a continuous metal film on an elastomeric substrate, bending deformation can

concentrate strain in the rigid Pt layer. The resulting cracks can open under bending stress and interrupt the conducting pathway, which explains the electrical failure observed for the Pt-TF electrode in the bent state in Fig. 6b. The recovery of resistance after release of bending stress can also be understood from this morphology. When the bending stress is removed, some crack faces or separated conducting regions can come back into contact, allowing the electrical pathway to be partially restored. Therefore, the Pt-TF electrode exhibits a reversible but deformation-dependent electrical response, which is not desirable for flexible electrodes that must operate under an applied bending state.

The 3D surface profiles in Fig. 7e and 7f further support the different deformation behaviors of the two electrodes. The corresponding surface roughness parameters obtained from 3D surface confocal laser scanning microscopy are summarized in Table 1. The Pt-NT electrode showed higher R_a, mean depth of hole, and mean height of peak values than the Pt-TF electrode. These values are mainly attributed to the intrinsic non-planar surface morphology of the embedded one-dimensional fibrous network rather than to catastrophic surface damage. In contrast, although the Pt-TF electrode showed a lower R_a value, its S_a value was higher than that of the Pt-NT electrode. Because S_a represents the areal roughness over the measured surface, the higher S_a value of the Pt-TF electrode indicates that crack formation caused larger surface irregularities over the electrode area after bending. Therefore, the Pt-NT electrode can be understood as having local topographical roughness arising from its fibrous architecture, whereas the Pt-TF electrode develops crack-induced areal surface damage during deformation. These results are consistent with the electrical responses in Fig. 6 and support the interpretation that the improved bending stability of the Pt-NT electrode originates from the preservation of the interconnected one-dimensional conducting network.

3.3. Application of Pt-NT electrodes to flexible piezoelectric devices

The applicability of the Pt-NT electrode as a deformable electrode was further examined by

integrating it into a flexible piezoelectric device. As schematically shown in Fig. 1b and 1d, the device was fabricated by combining the Pt-NT electrodes with a $BaTiO_3$-PDMS piezoelectric composite layer. The purpose of this device demonstration was not to optimize the energy harvesting performance but to verify whether the Pt-NT electrode could function as an electrically stable electrode in a mechanically deformable piezoelectric structure.

Fig. 8 shows the output current of the flexible piezoelectric device measured under periodic compressive loading with different applied forces and pushing frequencies. The output current increased with increasing applied force from 5 to 25 N. This behavior is attributed to the larger deformation of the $BaTiO_3$-PDMS composite layer under higher mechanical loading, which can generate a greater piezoelectric potential across the device. The output current also increased as the pushing frequency increased from 1 to 3 Hz. At higher frequencies, the repeated deformation of the piezoelectric composite occurs more rapidly, leading to a higher rate of charge generation and transfer through the external circuit.

The maximum output current reached approximately 40 nA under an applied force of 25 N at a pushing frequency of 3 Hz. Although this output level does not represent an optimized piezoelectric energy harvesting performance, the force- and frequency-dependent current response confirms that the Pt-NT electrode can collect and transmit piezoelectric charges generated from the BTO-PDMS composite layer under dynamic mechanical loading. Combined with the deformation reliability demonstrated in Fig. 6 and Fig. 7, these results indicate that the Pt-NT network electrode is a suitable deformable electrode platform for flexible piezoelectric devices.

4. Conclusion

In this study, PDMS-embedded Pt nanotube network electrodes were fabricated using a textured Si-assisted electrospinning/sputtering strategy. Electrospun PVP nanofibers formed on a textured Si wafer served as sacrificial one-dimensional templates for Pt deposition. Increasing the sputtering time

increased the diameter of the Pt-coated PVP nanofibers and reduced the sheet resistance, indicating the formation of electrically connected Pt pathways. After thermal treatment, the PVP template was removed while the interconnected Pt-based fibrous network was largely retained. The textured Si-assisted process also enabled the Pt-NT network to be embedded into PDMS, producing a flexible electrode architecture distinct from a conventional Pt thin film.

The Pt-NT electrode showed markedly improved electrical stability under mechanical deformation compared with the Pt-TF electrode. During bending, the Pt-NT electrode maintained electrical conduction in the bent state, whereas the Pt-TF electrode exhibited temporary electrical failure under bending stress. Under tensile stretching, the Pt-TF electrode failed above 20% strain, while the Pt-NT electrode retained conductive pathways even at 100% strain. Surface morphology and roughness analyses confirmed that the Pt-NT network suppressed crack-induced areal surface damage by preserving its interconnected one-dimensional architecture. In addition, the Pt-NT electrode was successfully applied to a $BaTiO_3$-PDMS flexible piezoelectric device, which generated an output current of approximately 40 nA under an applied force of 25 N at 3 Hz. These findings demonstrate that textured Si-assisted Pt-NT network electrodes are suitable deformable electrode platforms for flexible piezoelectric devices.

Acknowledgments

This work was supported by the Technology Innovation Program (RS-2025-16067075, Development of wet surface treatment technology for high strength metal-resin bonding in electric vehicle heater components) and by the Technology Innovation Program (RS-2024-00431424, Development of Ni-Cr-Mo based components and field application technology for semiconductor manufacturing process gas control with surface roughness < Ra 0.125 μm) funded by the Ministry of Trade, Industry and Resources (MOTIR, Korea).

References

[1] Y. Li, A. Veronica, J. Ma, H.Y.Y. Nyein, Materials, Structure, and Interface of Stretchable Interconnects for Wearable Bioelectronics. Adv. Mater. **37**(23), 2408456 (2025) https://doi.org/10.1002/adma.202408456

[2] J.A. Rogers, T. Someya, Y. Huang, Materials and Mechanics for Stretchable Electronics. Science **327**(5973), 1603-1607 (2010). https://doi.org/10.1126/science.1182383

[3] F.R. Fan, W. Tang, Z.L. Wang, Flexible Nanogenerators for Energy Harvesting and Self-Powered Electronics. Adv. Mater. **28**(22), 4283-4305 (2016) https://doi.org/10.1002/adma.201504299

[4] T. Cheng, Y. Zhang, W.-Y. Lai, W. Huang, Stretchable Thin-Film Electrodes for Flexible Electronics with High Deformability and Stretchability. Adv. Mater. **27**(22), 3349-3376 (2015) https://doi.org/10.1002/adma.201405864

[5] S. Yao, Y. Zhu, Nanomaterial-Enabled Stretchable Conductors: Strategies, Materials and Devices. Adv. Mater. **27**(9), 1480-1511 (2015) https://doi.org/10.1002/adma.201404446

[6] H.C. Ates, P.Q. Nguyen, L. Gonzalez-Macia, E. Morales-Narváez, F. Güder, J.J. Collins, C. Dincer, End-to-end design of wearable sensors. Nat. Rev. Mater. **7**, 887–907 (2022). https://doi.org/10.1038/s41578-022-00460-x

[7] J.-H. Lee, K.Y. Lee, M.K. Gupta, T.Y. Kim, D.-Y. Lee, J. Oh, C. Ryu, W.J. Yoo, C.-Y. Kang, S.-J. Yoon, J.-B. Yoo, S.-W. Kim, Highly Stretchable Piezoelectric-Pyroelectric Hybrid Nanogenerator. Adv. Mater. **26**(5), 765-769 (2014) https://doi.org/10.1002/adma.201303570

[8] H. Su, X. Wang, C. Li, Z. Wang, Y. Wu, J. Zhang, Y. Zhang, C. Zhao, J. Wu, H. Zheng, Enhanced energy harvesting ability of polydimethylsiloxane-$BaTiO_3$-based flexible piezoelectric nanogenerator for tactile imitation application. Nano Energy **83**, 105809 (2021) https://doi.org/10.1016/j.nanoen.2021.105809

[9] C. Cho, P. Kang, A. Taqieddin, Y. Jing, K. Yong, J.M. Kim, M.F. Haque, N.R. Aluru, S.W. Nam, Strain-resilient electrical functionality in thin-film metal electrodes using two-dimensional interlayers. Nat. Electron. **4**, 126–133 (2021) https://doi.org/10.1038/s41928-021-00538-4

[10] O. Graudejus, P. Görrn, S. Wagner, Controlling the morphology of gold films on poly(dimethylsiloxane). ACS Appl. Mater. Interfaces **2**(7), 1927–1933 (2010)

https://doi.org/10.1021/am1002537

[11] T. Baëtens, E. Pallecchi, V. Thomy, S. Arscott, Cracking effects in squashable and stretchable thin metal films on PDMS for flexible microsystems and electronics. Sci. Rep. **8**, 9492 (2018) https://doi.org/10.1038/s41598-018-27798-z

[12] C. Guo, T. Sun, Q. Liu, Z. Suo, Z. Ren, Highly stretchable and transparent nanomesh electrodes made by grain boundary lithography. Nat. Commun. **5**, 3121 (2014) https://doi.org/10.1038/ncomms4121

[13] R. Jiao, R. Wang, Y. Wang, Y.K. Cheung, X. Chen, X. Wang, Y. Deng, H. Yu, Vertical serpentine interconnect-enabled stretchable and curved electronics. Microsyst. Nanoeng. **9**, 149 (2023) https://doi.org/10.1038/s41378-023-00625-w

[14] D.S. Gray, J. Tien, C.S. Chen, High-Conductivity Elastomeric Electronics. Adv. Mater. **16**, 393–397 (2004) https://doi.org/10.1002/adma.200306107

[15] J. Lee, B. Llerena Zambrano, J. Woo, K. Yoon, T. Lee, Recent advances in 1D stretchable electrodes and devices for textile and wearable electronics: Materials, fabrications, and applications. Adv. Mater. **32**(5), 1902532 (2020) https://doi.org/10.1002/adma.201902532

[16] S. De, T.M. Higgins, P.E. Lyons, E.M. Doherty, P.N. Nirmalraj, W.J. Blau, J.J. Boland, J.N. Coleman, Silver Nanowire Networks as Flexible, Transparent, Conducting Films: Extremely High DC to Optical Conductivity Ratios. ACS Nano **3**(7), 1767–1774 (2009) https://doi.org/10.1021/nn900348c

[17] W.L. Hu, X.F. Niu, R. Zhao, Q.B. Pei, Elastomeric transparent capacitive sensors based on an interpenetrating composite of silver nanowires and polyurethane. Appl. Phys. Lett. **102**, 083303 (2013) https://doi.org/10.1063/1.4794143

[18] Y.-I. Lee, Study on the diameter-controlled synthesis of silver nanofibers and their application to transparent conductive electrodes. Korean J. Mater. Res. **25**(10), 537-542 (2015) https://doi.org/10.3740/MRSK.2015.25.10.537

[19] V.H. Nguyen, D.T. Papanastasiou, J. Resende, L. Bardet, T. Sannicolo, C. Jiménez, D. Muñoz-Rojas, N.D. Nguyen, D. Bellet, Advances in Flexible Metallic Transparent Electrodes. Small **18**, 2106006 (2022) https://doi.org/10.1002/smll.202106006

[20] S. Ye, A.R. Rathmell, Z. Chen, I.E. Stewart, B.J. Wiley, Metal Nanowire Networks: The Next Generation of Transparent Conductors. Adv. Mater. **26,** 6670-6687 (2014) https://doi.org/10.1002/adma.201402710

[21] R.M. Mutiso, M.C. Sherrott, A.R. Rathmell, B.J. Wiley, K.I. Winey, Integrating Simulations and Experiments To Predict Sheet Resistance and Optical Transmittance in Nanowire Films for Transparent Conductors. ACS Nano **7**(9), 7654–7663 (2013) https://doi.org/10.1021/nn403324t

[22] S. Gong, W. Schwalb, Y. Wang, Y. Chen, Y. Tang, J. Si, B. Shirinzadeh, W. Cheng, A wearable and highly sensitive pressure sensor with ultrathin gold nanowires. Nat. Commun. **5**, 3132 (2014) https://doi.org/10.1038/ncomms4132

[23] D.A. Smith, V.C. Holmberg, B.A. Korgel, Flexible Germanium Nanowires: Ideal Strength, Room Temperature Plasticity, and Bendable Semiconductor Fabric. ACS Nano **4**(4), 2356–2362 (2010) https://doi.org/10.1021/nn1003088

[24] S. Wang, Z. Shan, H. Huang, The Mechanical Properties of Nanowires. Adv. Sci. **4**(4), 1600332 (2017) https://doi.org/10.1002/advs.201600332

[25] P. Lee, J. Lee, H. Lee, J. Yeo, S. Hong, K.H. Nam, D. Lee, S.S. Lee, S.H. Ko, Highly Stretchable and Highly Conductive Metal Electrode by Very Long Metal Nanowire Percolation Network. Adv. Mater. **24**(25), 3326-3332 (2012) https://doi.org/10.1002/adma.201200359

[26] H. Lee, I. Kim, M. Kim, H. Lee, Moving beyond flexible to stretchable conductive electrodes using metal nanowires and graphenes. Nanoscale **8**(4), 1789–1822 (2016) https://doi.org/10.1039/c5nr06851g

[27] J.M. Kim, H.-I. Joh, S.M. Jo, D.J. Ahn, H.Y. Ha, S.-A. Hong, S.-K. Kim, Preparation and characterization of Pt nanowire by electrospinning method for methanol oxidation. Electrochim. Acta **55**(16), 4827-4835 (2010) https://doi.org/10.1016/j.electacta.2010.03.036

[28] Y.S. Kim, S.H. Nam, H.-S. Shim, H.-J. Ahn, M. Anand, W.B. Kim, Electrospun bimetallic nanowires of PtRh and PtRu with compositional variation for methanol electrooxidation. Electrochem. Commun. **10**(7), 1016-1019 (2008) https://doi.org/10.1016/j.elecom.2008.05.003

[29] D. Ji, Y. Lin, X. Guo, B. Ramasubramanian, R. Wang, N. Radacsi, R. Jose, X. Qin, S. Ramakrishna, Electrospinning of nanofibres. Nat. Rev. Methods Primers **4**, 1 (2024) https://doi.org/10.1038/s43586-023-00278-z

[30] H. Wu, D. Kong, Z. Ruan, P.-C. Hsu, S. Wang, Z. Yu, T. J. Carney, L. Hu, S. Fan, Y. Cui, A transparent electrode based on a metal nanotrough network. Nat. Nanotechnol. **8**, 421–425 (2013) https://doi.org/10.1038/nnano.2013.84

[31] J. Park, H.-J. Jeon, PDMS micro-dewy spider-web-like metal nanofiber films for fabrication of high-performance transparent flexible electrode with improved mechanical strength. Microelectron.

Eng. **258**, 111777 (2022) https://doi.org/10.1016/j.mee.2022.111777

[32] S. Lee, D. Sasaki, D. Kim, M. Mori, T. Yokota, H. Lee, S. Park, K. Fukuda, M. Sekino, K. Matsuura, T. Shimizu, T. Someya, Ultrasoft electronics to monitor dynamically pulsing cardiomyocytes. Nat. Nanotechnol. **14**, 156–160 (2019) https://doi.org/10.1038/s41565-018-0331-8

[33] S. Huang, Y. Liu, C.F. Guo, Z. Ren, A Highly Stretchable and Fatigue-Free Transparent Electrode Based on an In-Plane Buckled Au Nanotrough Network. Adv. Electron. Mater. **3**, 1600534 (2017) https://doi.org/10.1002/aelm.201600534

[34] C. Okutani, T. Yokota, T. Someya, Interconnected Heat-Press-Treated Gold Nanomesh Conductors for Wearable Sensors. ACS Appl. Nano Mater. **3**(2), 1848–1854 (2020) https://doi.org/10.1021/acsanm.9b02514

Table caption

Table 1 Surface roughness parameters of Pt-NT and Pt-TF electrodes after 1,000 cycles of bending, obtained by 3D surface confocal laser scanning microscopy

Figure captions

Fig. 1 Schematic illustration of **a** the formation of the Pt-NT network on a textured Si wafer, **b** an exploded schematic of the flexible piezoelectric device consisting of Pt-NT electrodes, **c** fabrication process of the Pt-NT network electrode, and **d** fabrication process of the flexible piezoelectric device

Fig. 2 FE-SEM images of **a, e** electrospun PVP nanofibers and Pt-coated PVP nanofibers sputtered for **b, f** 10 min, **c, g** 20 min, and **d, h** 30 min

Fig. 3 Size distributions of **a** electrospun PVP nanofibers and Pt-coated nanofibers sputtered for **b** 10 min, **c** 20 min, and **d** 30 min. **e** Average nanofiber diameter (black squares) and sheet resistance (red circles) as a function of Pt sputtering time

Fig. 4 FE-SEM images and EDS mapping images of Pt-coated PVP nanofiber networks on a textured Si wafer: **a-f** before and **g-l** after thermal treatment at 500 °C for 3 h. **a, g** Top-view FE-SEM images with corresponding EDS mapping images of **b, h** Si and **c, i** Pt; **d, j** side-view FE-SEM images with corresponding EDS mapping images of **e, k** Si and **f, l** Pt

Fig. 5 FE-SEM images and EDS mapping images of the fabricated electrodes: **a-d** PDMS-embedded Pt-NT electrode and **e-h** Pt-TF electrode prepared by direct Pt sputtering on PDMS for 30 min. Corresponding EDS maps of **c, g** Si and **d, h** Pt. Insets in **a** and **e** show digital photographs of the respective electrodes

Fig. 6 Electrical stability of Pt-NT and Pt-TF electrodes under mechanical deformation: cyclic

bending responses of **a** the Pt-NT electrode and **b** the Pt-TF electrode measured in the bent and released states, and **c** resistance variation as a function of tensile strain

Fig. 7 Surface morphology and roughness analyses of Pt-NT and Pt-TF electrodes after the bending test of 1,000 cycles in the released state: FE-SEM images of the Pt-NT electrode **a** before and **b** after bending, FE-SEM images of the Pt-TF electrode **c** before and **d** after bending, and 3D confocal laser scanning microscopy images of **e** the Pt-NT electrode and **f** the Pt-TF electrode after bending

Fig. 8 Piezoelectric output current of the flexible device using Pt-NT electrodes measured under periodic compressive loading with applied forces of 5 to 25 N and pushing frequencies of **a** 1, **b** 2, and **c** 3 Hz

Table

Table 1 Surface roughness parameters of Pt-NT and Pt-TF electrodes after 1,000 cycles of bending, obtained by 3D surface confocal laser scanning microscopy

Samples	Mean depth of hole (μm)	Mean height of peak (μm)	R_a (μm)	S_a (μm)
Pt-NT electrode	0.427	0.421	0.327	0.677
Pt-TF electrode	0.273	0.220	0.099	0.866

Figures

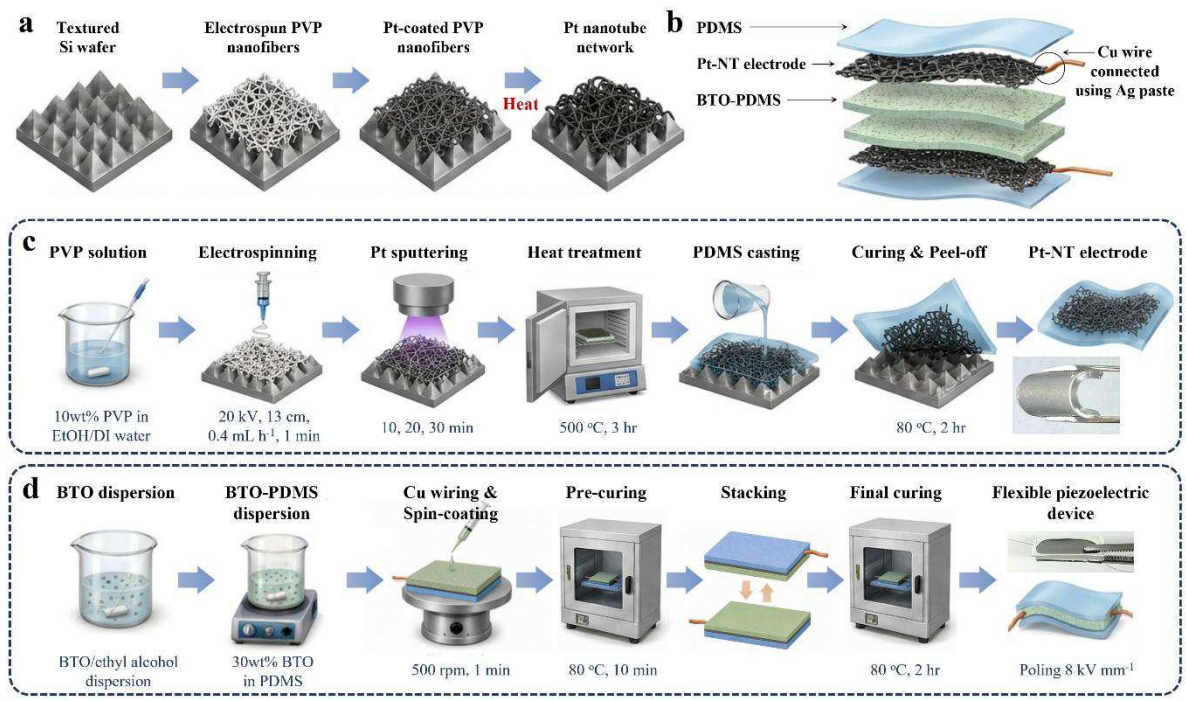


Fig. 1 Schematic illustration of **a** the formation of the Pt-NT network on a textured Si wafer, **b** an exploded schematic of the flexible piezoelectric device consisting of Pt-NT electrodes, **c** fabrication process of the Pt-NT network electrode, and **d** fabrication process of the flexible piezoelectric device

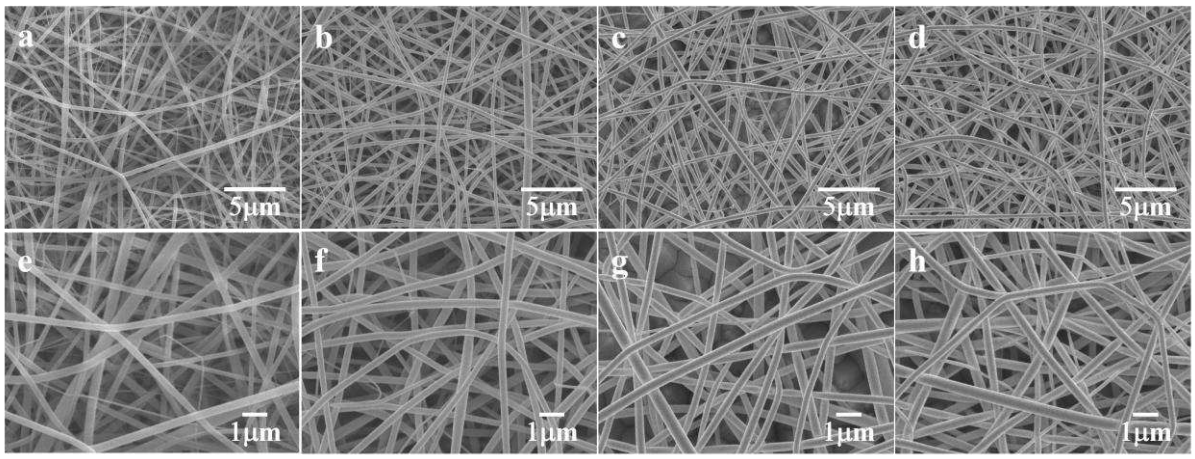


Fig. 2 FE-SEM images of **a, e** electrospun PVP nanofibers and Pt-coated PVP nanofibers sputtered for **b, f** 10 min, **c, g** 20 min, and **d, h** 30 min

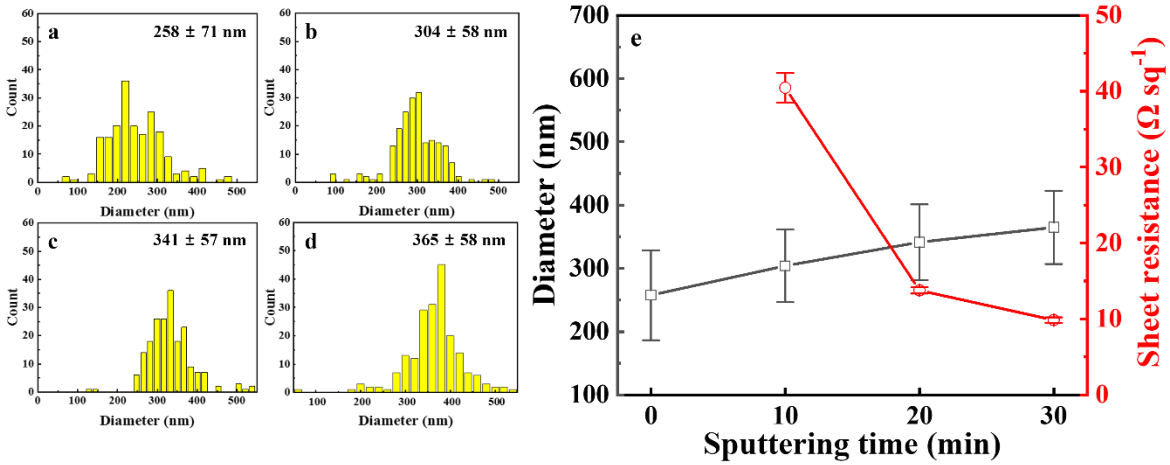


Fig. 3 Size distributions of **a** electrospun PVP nanofibers and Pt-coated nanofibers sputtered for **b** 10 min, **c** 20 min, and **d** 30 min. **e** Average nanofiber diameter (black squares) and sheet resistance (red circles) as a function of Pt sputtering time

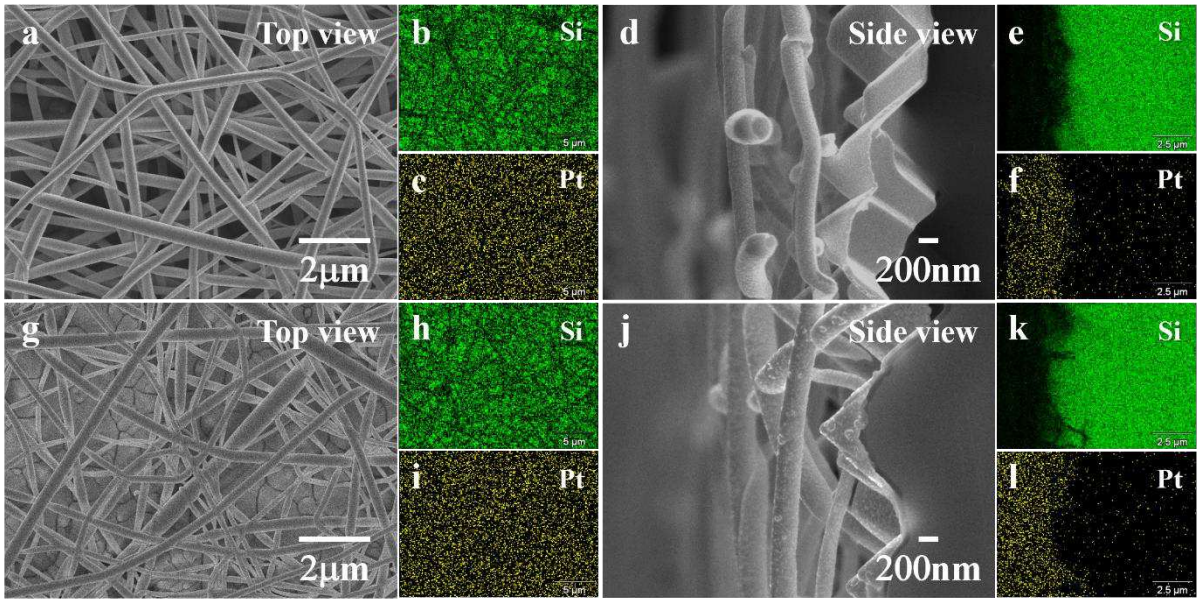


Fig. 4 FE-SEM images and EDS mapping images of Pt-coated PVP nanofiber networks on a textured Si wafer: **a-f** before and **g-l** after thermal treatment at 500 °C for 3 h. **a, g** Top-view FE-SEM images with corresponding EDS mapping images of **b, h** Si and **c, i** Pt; **d, j** side-view FE-SEM images with corresponding EDS mapping images of **e, k** Si and **f, l** Pt

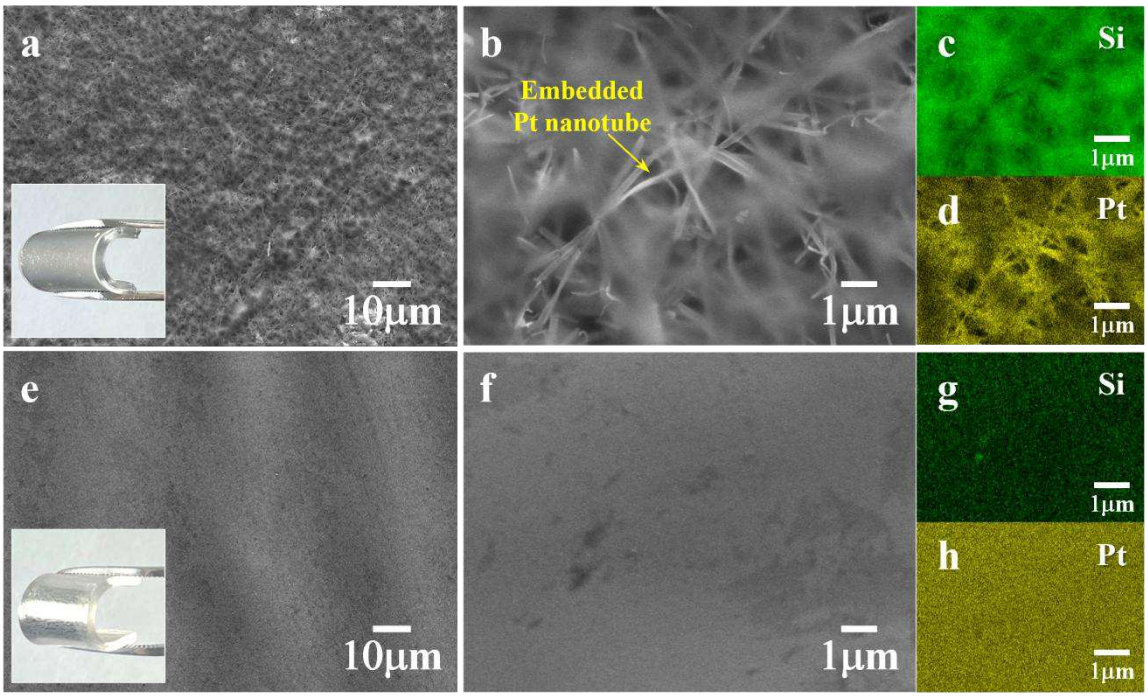


Fig. 5 FE-SEM images and EDS mapping images of the fabricated electrodes: **a-d** PDMS-embedded Pt-NT electrode and **e-h** Pt-TF electrode prepared by direct Pt sputtering on PDMS for 30 min. Corresponding EDS maps of **c, g** Si and **d, h** Pt. Insets in **a** and **e** show digital photographs of the respective electrodes

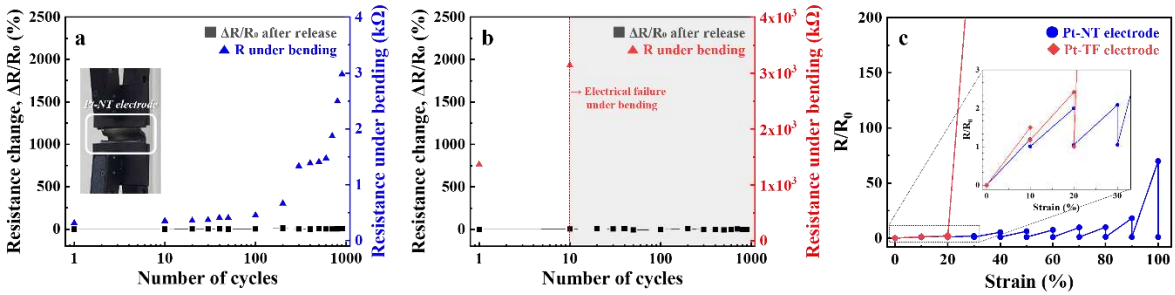


Fig. 6 Electrical stability of Pt-NT and Pt-TF electrodes under mechanical deformation: cyclic bending responses of **a** the Pt-NT electrode and **b** the Pt-TF electrode measured in the bent and released states, and **c** resistance variation as a function of tensile strain

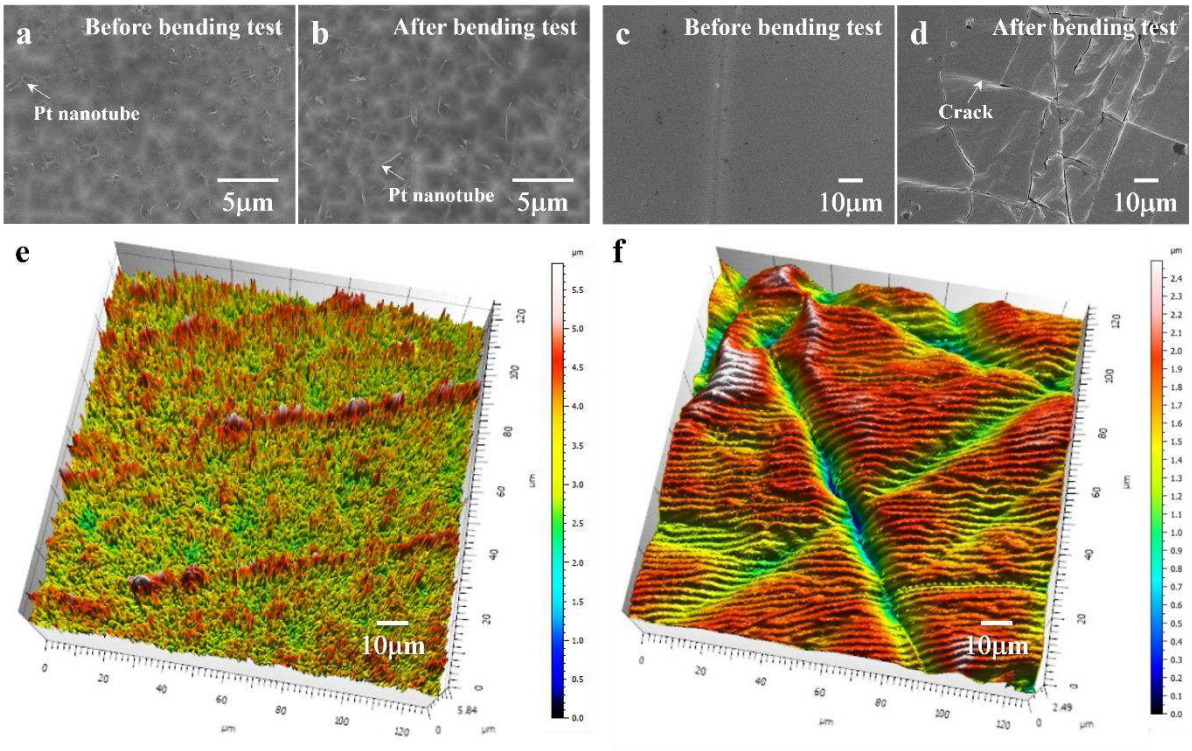


Fig. 7 Surface morphology and roughness analyses of Pt-NT and Pt-TF electrodes after the bending test of 1,000 cycles in the released state: FE-SEM images of the Pt-NT electrode **a** before and **b** after bending, FE-SEM images of the Pt-TF electrode **c** before and **d** after bending, and 3D confocal laser scanning microscopy images of **e** the Pt-NT electrode and **f** the Pt-TF electrode after bending

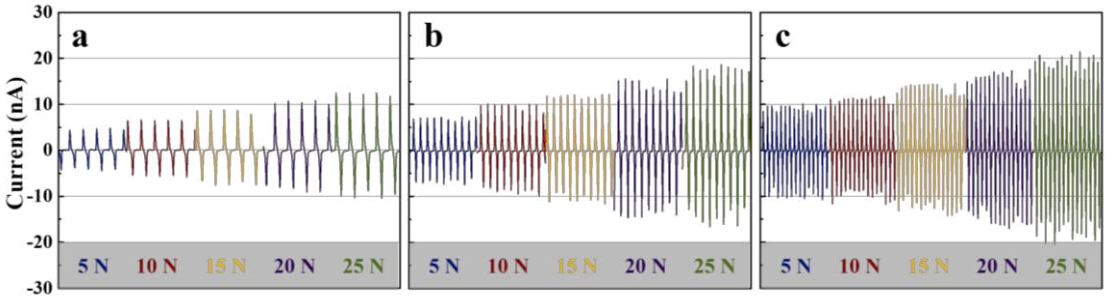


Fig. 8 Piezoelectric output current of the flexible device using Pt-NT electrodes measured under periodic compressive loading with applied forces of 5 to 25 N and pushing frequencies of **a** 1, **b** 2, and **c** 3 Hz